Circuit Model for Graphene Screen-Printed Films

Fabio Peinetti, Simone Quaranta, and Patrizia Savi

Abstract — Graphene flakes can be screen printed on different substrates through the preparation of inks with a proper combination of solvents and binders. In this article, an equivalent lumped circuit model of a graphene film is obtained by fitting the measured scattering parameters of graphene-loaded microstrip lines with Cadence AWR software simulations.

1. Introduction

Films loaded with graphene nanoplatelets (GNPs) have gained great attention in recent decades. Through the preparation of inks with a proper combination of solvents and binders [1], films can be deposited on different substrates. The main techniques to deposit films are blade coating, inkjet [2, 3], and screen printing, as described in detail in [4]. Each technique requires proper ink preparation [5]. In particular, screen printing calls for quite viscous and thixotropic pastes. Therefore, a certain amount of binder or rheology modifier needs to be added to the paste formulation. Hence, the binder cannot be completely removed by thermal treatment when screen printing is performed on polymer-based substrates. Graphene films are used in many applications in the optical [6], RF, and millimeter-wavelength range as gas sensors [7], humidity sensors [8, 9], glucose sensors [10, 11], tunable devices [12, 13], flexible electronics [14, 15], and electromagnetic (EM) absorbers [16]. For films loaded with graphene, even if in many applications a graphene film can be easily described by using its sheet resistance, a customized model should be introduced to account for all the substances present in the deposition [17]. For sensing applications, characterization of graphene-based films with an electric equivalent circuit and knowledge of the variation of the circuit parameters due to interaction with the target molecules is helpful. Consequently, knowledge of the EM properties of graphene at microwave frequency is crucial. However, there has been little research on the characterization of graphene films at microwave frequencies [18]. The circuit models at microwave frequency are generally based on series or parallel *RLC* resonators. In [16, 19], the authors introduce two models to describe graphene inks below (Davidson–Cole model) and above (Lorentz model) the percolation threshold. Two types of GNP-based inks were tested with 8 wt% and 12 wt% of polymethyl methacrylate in solution with an organic solvent. An equivalent circuit of the polyaniline polimeric matrix (PANI) and graphene nanocomposites formed by a parallel of a capacitor and a resistor, plus a series resistance taking into account the PANI, is introduced in [20].

In this article, a description of graphene films with a lumped circuit model is introduced, and the binder and graphene are individually modeled. The model is obtained by fitting, in the microwave range, measured *S* parameters on AWR Microwave Office software (version 22.1). Starting from the preliminary model described in [21], the binder and the GNPs are individually modeled. In the enhanced model of this work, the fitting of the parameters is greatly improved over the frequency range, and many circuit elements are added to deal with microscopic effects taking place at microwave frequency. The proposed equivalent lumped circuit model proves suitable as an initial step toward the full-wave EM modeling and analysis of graphene-loaded microwave structures intended for sensing and tuning applications.

In Section 2, the microstrip circuit and film deposition are described. Section 3.1 deals with the model of the gap filled with a binder: ethyl cellulose (EC) film. In Section 3.2, the model of the film loaded with graphene flakes of weight fractions of 25% and 33% is introduced. In Section 4, the measured *S* parameters of the microstrip lines with binder alone and with graphene films are compared with the results obtained by the model.

2. Microstrip Lines and Film Deposition

To obtain a circuit model of a film loaded with graphene, a simple microstrip line with a gap is considered (Figure 1). Across the gap, the ink with the chosen composition of graphene is deposited by a screen-printing technique. In this work, graphene nanoplates are used with weight fractions of 25% and 33%. Screen-printing paste was made of EC (viscosity 10 cP, 5% toluene–ethanol, and 48% ethoxyl) binder–stabilizer, α-terpineol solvent, and graphene flakes as the active ingredients. Component ratio (weight percent) was 9.5:65.5:25, respectively. All components were mixed in ethanol stirred for 2 h and finally sonicated with a titanium horn for 15 h. Ethanol was removed by rotary evaporation to attain a printable paste. Ink was deposited layer by layer with a 90 T polyester screen-printing mesh. Three layers were sequentially printed onto an FR4 substrate achieve a 30 μm film thickness. Film dimensions measured up to 3 mm × 3 mm. The coating was dried at 125 °C for 2.5 h [22].

Manuscript received 17 February 2023.

Fabio Peinetti and Patrizia Savi are with the Department of Electronics and Telecommunications, Politecnico di Torino, Corso Duca degli Abruzzi, 24, 10129 Torino, Italy; e-mail: fabio.peinetti@polito.it, patrizia.savi@polito.it.

Simone Quaranta is with the Consiglio Nazionale delle Ricerche, Institute for the Study of Nanostructured Materials, Piazzale Aldo Moro, 5, 00185 Roma, Italy; e-mail: simone.quaranta@cnr.it.

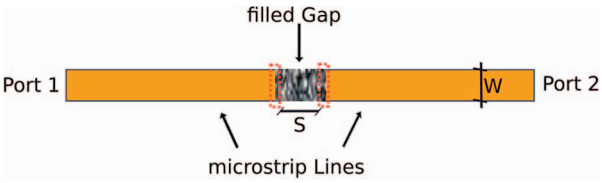

Figure 1. Top view of the microstrip line with a centered gap.

3. Circuit Model of the Film

First of all, instead of using the default microstrip gap element (MGAP) available in AWR software with discrete components [23], a specific model of the gap is developed to obtain a better description of the percolative paths and dielectric loss. Furthermore, a series resistance (R_s) successfully models the sheet resistance, measured in [7]. First, a model for the binder alone, EC, is developed (see Section 3.1). Based on this preliminary analysis, the final model describing the behavior of a graphene film with a weight fraction of 25% is derived (see Section 3.2).

3.1 Binder-Filled Gap Model

The default MGAP available in AWR software has some limitations on the dimensions of the gap ($0.1 < S/H < 1$, $0.5 < W/H < 2.5$) [23, 24]. To describe a gap with a geometry not included in the previously cited range (in our case $S/H = 1.65$ and $W/H = 1.9$; see Section 4), a new model of the binder-filled gap is introduced (see Figure 2). The red-squared box is the *core*, which is modified to fit graphene deposition's S parameters (see Section 3.2) by adding other circuit elements. For the classical model, made up of a capacitive pi network [24], series resistors are added. A further variation includes the presence of an inductive element. In Figure 2, the transmission lines connected to port 1 and port 2 are not shown. The inner capacitors toward ground (C_{gl}, C_{gr}) model the parallel plate capacitance between the microstrip connected to port 1 and port 2 and the ground plane, in correspondence to the gap. On the other hand, C_g accounts for the capacitance between the two lines, separated by the dielectric binder; the C_g value is about eight times lower than the capacitances C_{gl}, C_{gr} (Table 1). We consider $C_{gl} = C_{gr}$. R_g, R_{gl}, and R_{gr} account for losses in the dielectric at high frequency. Due to the high loss tangent, the corresponding resistance is on the order of one hundred ohms. The resistor, named R_s in Figure 2, represents the sheet resistance and models the percolative path in the EC filler. Because the binder matrix is basically dominated by the dielectric compound, the low efficient electron tunneling causes R_s to be large, namely, 34 kΩ. As pointed out in several works [21, 22], the real part of the impedance is influenced by variations in the actual composition of the compound: an increase in the graphene weight fraction corresponds to a reduction of the resistance and vice versa.

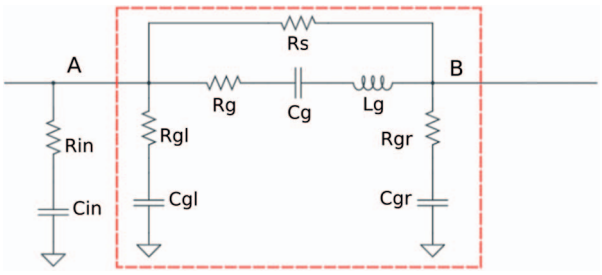

Figure 2. Binder-filled gap circuit.

Table 1. Binder electrical model parameters

Parameter (unit)	Value
R_s (kΩ)	34
R_g (kΩ)	2.98
C_g (pF)	0.0107
L_g (pH)	15.8
R_{gl} (Ω)	91
C_{gl} (pF)	0.085
R_{gr} (Ω)	91
C_{gr} (pF)	0.085
R_{in} (Ω)	3.4
C_{in} (pF)	0.38
R_{out} (Ω)	—
C_{out} (pF)	—
C_{pp} (pF)	—

3.2 Graphene-Filled Gap Model

In this section, the graphene weight fractions of 25% and 33% film deposition are analyzed. Because graphene ink requires an adhesion element, such as EC, to be printed and due to the impossibility to remove the binder, even with thermal treatment, the developed model accounts for both the effects of graphene and EC, which is the reason a model for the binder was developed (see Section 3.1). The circuital topology of

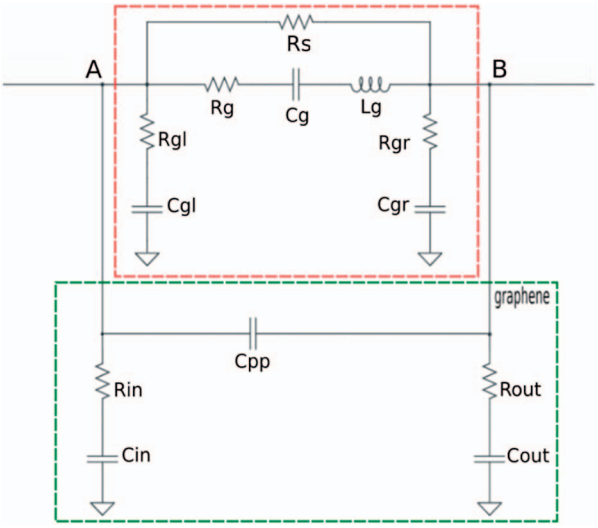

Figure 3. Graphene-filled gap circuit.

Table 2. Graphene weight fraction (25%) electrical model parameters

Parameter (unit)	Value
R_s (kΩ)	0.425
R_g (kΩ)	1
C_g (pF)	0.032
L_g (pH)	15.8
R_{gl} (Ω)	28
C_{gl} (pF)	0.085
R_{gr} (Ω)	28
C_{gr} (pF)	0.085
R_{in} (Ω)	36
C_{in} (pF)	0.2
R_{out} (Ω)	36
C_{out} (pF)	0.2
C_{pp} (pF)	0.029

Figure 2 can be found in Figure 3 (red box), too. However, circuit parameters are changed to properly fit chemically different EC–graphene deposition as reported in Tables 2 and 3. Moreover, some components, placed inside the green box, are added to improve the *S*-parameters fitting. In particular, the parallel capacitor C_{pp} accounts for the creation of nanoscale capacitors, whose conductive element is the graphene platelet and the binder acts as dielectric material [21]. Moreover, an *RC* series element is added at the output node, making the circuit symmetric ($R_{in} = R_{out}$, $C_{in} = C_{out}$). The increase in percolative paths is linked to a reduction in resistive elements and, in particular in R_s, which falls from 34 kΩ to 425 Ω. The comparison of Tables 1 and 2 shows that also the other resistors are strongly decreased. The same reasoning applies when increasing the graphene weight fraction up to (33%); in this case, R_s is further reduced to 207 Ω (Table 3). The value of R_s can be used to evaluate the sheet resistance defined as

$$R_{sheet} = R_s \frac{W}{S} \tag{1}$$

The resulting sheet resistance is 425 Ω/sq, using a unitary aspect ratio. The calculated value is the DC resistance between node A and node B, and it is very close to the measured value, namely, 440 Ω/sq, obtained in [21] with the same type of deposition. The inductance L_g, C_{gl}, and C_{gr} are left unaltered, as shown in Tables 1 and 2 by comparison.

Table 3. Graphene weight fraction (33%) electrical model parameters

Parameter (unit)	Value
R_s (kΩ)	0.207
R_g (kΩ)	1
C_g (pF)	0.032
L_g (pH)	15.8
R_{gl} (Ω)	28
C_{gl} (pF)	0.085
R_{gr} (Ω)	28
C_{gr} (pF)	0.085
R_{in} (Ω)	81
C_{in} (pF)	0.216
R_{out} (Ω)	71
C_{out} (pF)	0.22
C_{pp} (pF)	0.24

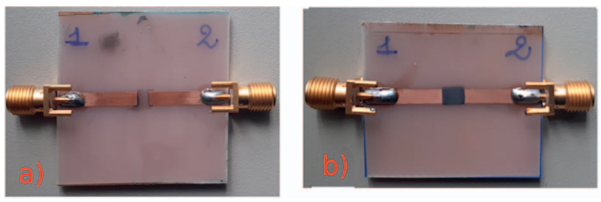

Figure 4. Microstrip with unfilled gap (a) and filled with graphene-based ink (b).

4. Results

A 35 mm long copper microstrip line, corresponding to 50 Ω, was etched on FR4 substrate of thickness $H = 1.57$ mm, $\varepsilon_r = 3.9$, $\tan\delta = 0.03$, $\rho_{FR4} = 17.24$ mΩ μm. The width (W) of the microstrip line was chosen to be 3 mm to have a 50 Ω impedance. A gap of length $S =$ 2.6 mm was left in the middle to host the graphene film (see Figure 1). The size of the deposition was 3 mm × 3 mm, because 0.2 mm was overimposed on the lines on each side to guarantee an electric connection (see Figure 4). Three types of microstrip circuits were manufactured: one with an ink made with the binder alone and the other two with a deposition of two layers of graphene of 25 wt% ink and 33 wt%. The scattering parameters of the microstrip lines with the film (binder alone and binder with graphene) were measured with a two-port Vector Network Analyzer by Keysight (P9372A) from 200 MHz to 4.5 GHz. Figure 5 shows the simulated S_{21} (solid lines), compared with the measured one (dashed lines) for the unfilled gap. The *S* parameters remain unchanged when the gap is binder filled because the relative dielectric constant and the loss tangent of the cellulose derivative binders are of the same order of FR4. The circuit parameters

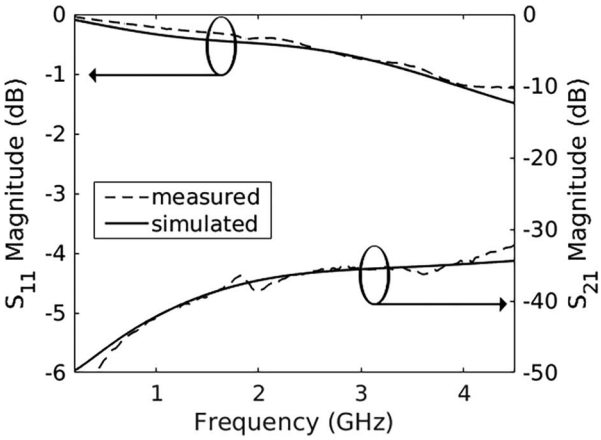

Figure 5. Binder-filled gap: measured reflection and transmission coefficient (dashed line) and simulated (solid line).

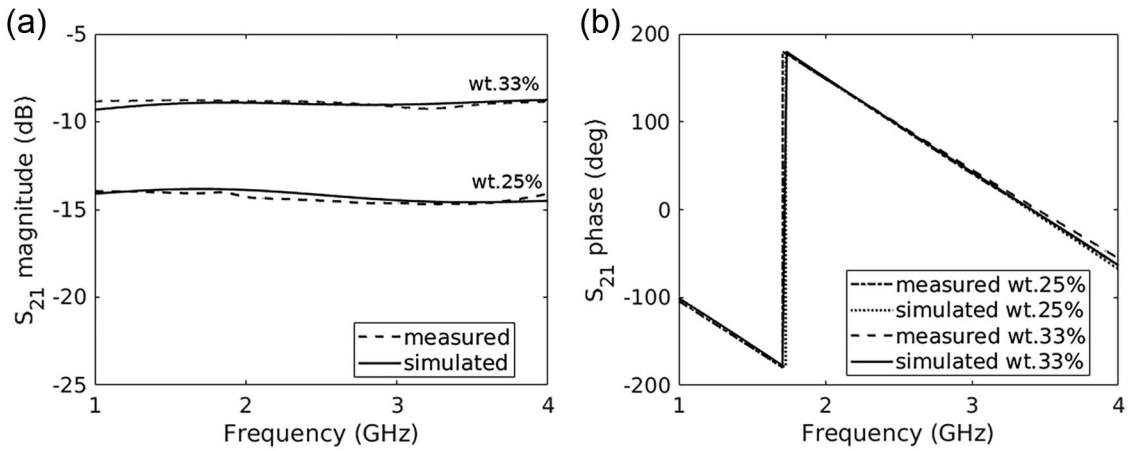

Figure 6. Graphene-filled gap (25 wt% and 33 wt%): measured transmission coefficient (dashed line) and simulated (solid line). (a) Magnitude; (b) phase.

used in the simulation are reported in Table 1. The S parameters (S_{12} and S_{22}) are not plotted because they are close to S_{21} and S_{11}, respectively. Measured (dashed line) and model-derived fitted data (solid line) of the transmission coefficient are compared in Figure 6 for the graphene-filled gap (25 wt% and 33 wt%). Both magnitude and phase are analyzed. No phase differences can be appreciated between the two percentages of graphene, while a reduction (absolute value) in S_{21} can be observed when increasing the graphene weight fraction. This effect may be due to the increase in percolative paths, confirmed by a reduction in the sheet resistance.

Even if not reported, as expected from the previous result, S_{11} decreases when increasing the weight fraction. Overall, good agreement is observed between the measurements and the circuit model over the range 200 MHz to 4.5 GHz. Between the measured data and the fitted data, a difference lower than 1 dB is obtained for both the transmission coefficient (Figure 3) and the reflection coefficient (not reported here). The results obtained in this work and the results of other graphene-based ink depositions made with the screen-printing technique are listed in Table 4. The values of DC sheet resistance, modeled (Z_{sim}, corresponding to R_s in Figure 3) and measured (Z_{meas}), are not directly comparable because the composition of the inks, annealing temperature, and thicknesses are different. A common feature is that the sheet resistance values decrease with the increase of the weight percent of GNPs. In [16, 19], the sheet resistance of GNPs inks with different graphene weight fractions is compared in the microwave range. It is shown that the screen-printed number of layers influences the electrical properties as well. Graphene percentages taken into account in [19] are lower than those analyzed in this article, leading to much higher resistive effects.

5. Conclusion

A microstrip line loaded with a graphene insert was fabricated by screen printing and modeled through a lumped element circuit. Specifically, binder only (EC) and graphene-loaded (25 wt%) were printed on FR4 substrates. Electromagnetic behavior of both films was simulated with AWR software in the 200 MHz to 4.5 GHz range. Measured scattering parameters were fitted by means of *RC* series groups. The additional parallel capacitance inserted in the graphene film model can be ascribed to nonideal (i.e., leaky) nano-capacitances stemming from the graphene–binder interaction. Simulated and experimental results were found to be in accordance with each other (less than 1 dB difference throughout the entire frequency range). This equivalent lumped circuit can be extended to characterize films with different graphene loading. Furthermore, it can be improved and used in full-wave EM simulations to analyze sensing or tunable devices, where graphene is currently modeled by a simple sheet resistance.

Table 4. Overview of other works based on graphene ink

Ink type	Thickness (μm)	Weight percent	Z_{sim} (Ω) [source]	Z_{meas} (Ω) [source]	Temperature (°C)
EC + terpineol	20	33	207 [this work]	110 [22]	130
EC + terpineol	20	25	425 [this work]	440 [22]	130
Copolimer	40	25		30 [25]	100
Polymethyl methacrylate + organic solvent	20	14		180 [19]	260

6. References

1. W. J. Hyun, E. B. Secor, M. C. Hersam, C. D. Frisbie, and L. F. Francis, "High-Resolution Patterning of Graphene by Screen Printing With a Silicon Stencil for Highly Flexible Printed Electronics," *Advanced Materials*, **27**, 1, January 2015, pp. 109-115.
2. A. Chiolerio, G. Maccioni, P. Martino, M. Cotto, P. Pandolfi, et al., "Inkjet Printing and Low Power Laser Annealing of Silver Nanoparticle Traces for the Realization of Low Resistivity Lines for Flexible Electronics," *Microelectronic Engineering*, **88**, 8, August 2011, pp. 2481-2483.
3. E. B. Secor, L. P. Prabhumirashi, K. Puntambekar, M. L. Geier, and M. C. Hersam, "Inkjet Printing of High Conductivity, Flexible Graphene Patterns," *The Journal of Physical Chemistry Letters*, **4**, 8, April 2013, pp. 1347-1351.
4. T. S. Tran, N. K. Dutta, and N. R. Choudhury, "Graphene Inks for Printed Flexible Electronics: Graphene Dispersions, Ink Formulations, Printing Techniques and Applications," *Advances in Colloid and Interface Science*, **261**, November 2018, pp. 41-61.
5. A. C. M. De Moraes, J. Obrzut, V. K. Sangwan, J. R. Downing, L. E. Chaney, et al., "Elucidating Charge Transport Mechanisms in Cellulose-Stabilized Graphene Inks," *Journal of Materials Chemistry C*, **8**, 43, August 2020, pp. 15086-15091.
6. F. Bonaccorso, Z. Sun, T. Hasan, and A. C. Ferrari, "Graphene Photonics and Optoelectronics," *Nature Photonics*, **4**, 9, September 2010, pp. 611-622.
7. P. Savi, K. Naishadham, S. Quaranta, M. Giorcelli, and A. Bayat, "Microwave Characterization of Graphene Films for Sensor Applications," IEEE International Instrumentation and Measurement Technology Conference, Torino, Italy, May 22–25, 2017, pp. 1-6.
8. D. Lei, Q. Zhang, N. Liu, T. Su, L. Wang, et al., "Self-Powered Graphene Oxide Humidity Sensor Based on Potentiometric Humidity Transduction Mechanism," *Advanced Functional Materials*, **32**, 10, March 2022, p. 2107330.
9. X. Leng, W. Li, D. Luo, and F. Wang, "Differential Structure With Graphene Oxide for Both Humidity and Temperature Sensing," *IEEE Sensors Journal*, **17**, 14, June 2017, pp. 4357-4364.
10. Z. Zhu, L. Gancedo, A. J. Flewitt, H. Xie, F. Moussy, et al., "A Critical Review of Glucose Biosensors Based on Carbon Nanomaterials: Carbon Nanotubes and Graphene," *Sensors*, **12**, 5, May 2012, pp. 5996-6022.
11. R. Reghunath and K. K. Singh, "Recent Advances in Graphene Based Electrochemical Glucose Sensor," *Nano-Structures & Nano-Objects*, **26**, 2, April 2021, p. 100750.
12. M. Bozzi, L. Pierantoni, and S. Bellucci, "Applications of Graphene at Microwave Frequencies," *Radioengineering*, **24**, 3, September 2015, pp. 661-669.
13. M. Qu, J. Song, L. Yao, S. Li, L. Deng, et al., "Design of a Graphene-Based Tunable Frequency Selective Surface and Its Application for Variable Radiation Pattern of a Dipole at Terahertz," *Radio Science*, **53**, 2, February 2018, pp. 183-189.
14. M. Yasir, S. Bistarelli, A. Cataldo, M. Bozzi, L. Perregrini, et al., "Enhanced Tunable Microstrip Attenuator Based on Few Layer Graphene Flakes," *IEEE Microwave and Wireless Components Letters*, **27**, 4, March 2017, pp. 332-334.
15. S. G. Wallace, M. C. Brothers, Z. E. Brooks, S. V. Rangnekar, D. Lam, et al. "Fully Printed and Flexible Multi-Material Electrochemical Aptasensor Platform Enabled by Selective Graphene Biofunctionalization," *Engineering Research Express*, **4**, 1, March 2022, p. 015037.
16. M. Olszewska-Placha, B. Salski, D. Janczak, P. R. Bajurko, W. Gwarek, et al., "A Broadband Absorber With a Resistive Pattern Made of Ink With Graphene Nano-Platelets," *IEEE Transactions on Antennas and Propagation*, **63**, 2, December 2014, pp. 565-572.
17. D. S. L. Abergel, V. Apalkov, J. Berashevich, K. Ziegler, and T. Chakraborty, "Properties of Graphene: A Theoretical Perspective," *Advances in Physics*, **59**, 4, August 2010, pp. 261-482.
18. M. Liang, M. Tuo, S. Li, Q. Zhu, and H. Xin, "Graphene Conductivity Characterization at Microwave and THz Frequency," 8th European Conference on Antennas and Propagation, The Hague, Netherlands April 6–11, 2014, pp. 489-491.
19. P. Kopyt, B. Salski, P. Zagrajek, D. Janczak, M. Sloma, et al., "Electric Properties of Graphene-Based Conductive Layers From DC Up To Terahertz Range," *IEEE Transactions on Terahertz Science and Technology*, **6**, 3, May 2016, pp. 480-490.
20. A. Chiolerio, S. Porro, and S. Bocchini, "Impedance Hyperbolicity in Inkjet-Printed Graphene Nanocomposites: Tunable Capacitors for Advanced Devices," *Advanced Electronic Materials*, **2**, 3, March 2016, p. 1500312.
21. O. Sanusi, P. Savi, S. Quaranta, A. Bayat, and L. Roy, "Equivalent Circuit Microwave Modeling of Graphene-Loaded Thick Films Using *S*-Parameters," *Progress in Electromagnetics Research Letters*, **76**, May 2018, pp. 33-38.
22. S. Quaranta, M. Miscuglio, A. Bayat, and P. Savi, "Morphological and Radio Frequency Characterization of Graphene Composite Films," *C Journal of Carbon Research*, **4**, 2, May 2018, pp. 32-44.
23. *AWR Microwave Office Element Catalog*, version 22.1, San Jose, CA, USA, Cadence Design Systems, https://kb.awr.com/display/awrfaq/Documentation?preview=%2F11894861%2F93356088%2FMWO_AO_Elements_v22_1.pdf&searchId=VXW417SI0, 2022.
24. N. H. L. Koster and R. H. Jansen, "The Equivalent Circuit of the Asymmetrical Series Gap in Microstrip and Suspended Substrate Lines," *IEEE Transactions on Microwave Theory and Techniques*, **30**, 8, August 1982, pp. 1273-1279.
25. K. Arapov, E. Rubingh, R. Abbel, J. Laven, G. de With, et al., "Conductive Screen Printing Inks by Gelation of Graphene Dispersions," *Advanced Functional Materials*, **26**, 4, January 2016, pp. 586-593.